cancers

MDPI

Article

PEERing into the Future: Benchmarking the ANSTO Australian Synchrotron's Very-High-Energy Electron Linac for Ultra-High Dose-Rate, In Vivo FLASH Radiotherapy Research

James Cayley [1,*,†], Elette Engels [1,2,3,*,†], Tessa Charles [2], Kiarn Roughley [1], Marie Wegner [4], Sarah Koschny [1], Kirsty Brunt [2], Matthew Cameron [2], Daniel Hausermann [2], Paul Bennetto [2], Elisabetta Gargioni [5], Moeava Tehei [1], Elisabeth Schültke [6], Anatoly Rosenfeld [1], Yaw-Ren Eugene Tan [2,‡] and Michael Lerch [1,‡]

1 Centre for Medical Radiation Physics, University of Wollongong, Wollongong, NSW 2522, Australia
2 Australian Synchrotron, Australian Nuclear Science and Technology Organisation, Melbourne, VIC 3168, Australia; bruntk@ansto.gov.au (K.B.); yawrent@ansto.gov.au (Y.-R.E.T.)
3 Peter MacCallum Cancer Centre and University of Melbourne Sir Peter MacCallum Department of Oncology, Melbourne, VIC 3165, Australia
4 Institute of Product Development and Mechanical Engineering Design, Hamburg University of Technology, 21073 Hamburg, Germany
5 Department of Radiotherapy and Radiation Oncology, University Medical Center Hamburg-Eppendorf, 20246 Hamburg, Germany; e.gargioni@uke.de
6 Department of Radiooncology, Rostock University Medical Center, 18059 Rostock, Germany
* Correspondence: jcayley@uow.edu.au (J.C.); elette@uow.edu.au (E.E.)
† These authors contributed equally to this work.
‡ These authors contributed equally to this work.

Simple Summary

The field of radiotherapy is continually advancing, striving for ways in which to deliver a dose to a tumour while limiting the damage to nearby tissues. An increasingly common technique which is under intense development is that of FLASH radiotherapy, where doses are often delivered in fractions of seconds, rather than multiple deliveries over the span of weeks and months. Recent investigations have combined this technique with very-high-energy electrons to also target deep-seated tumours. There are a limited number of facilities available globally to undertake these investigations. This study demonstrates the successes of a new facility in Australia, suitable for such work.

Abstract

Background/Objectives: The PEER beamline at the ANSTO Australian Synchrotron has been developed to enable VHEE FLASH radiotherapy studies, both dosimetric and biological. Featuring a 100 MeV electron linac, it delivers single or multi-pulse irradiations consisting of 100 ps bunches with a 2 ns spacing, resulting in average dose-rates and instantaneous dose-rates as high as 10^8 Gy/s and 10^9 Gy/s, respectively. Much work has been conducted to realise a stable accelerator facility, complete with the tooling and diagnostics required to undertake such studies. However, to truly confirm its suitability required a successful biological benchmarking. **Methods:** Three cell lines were irradiated utilising real-time dosimetry to compare linear quadratic cell survival curves with other facilities. Also, mouse cadavers were transported and irradiated, mimicking live animals, to assess the feasibility and logistics of small animal experiments. **Results:** By comparing the trends of the linear quadratic model, evident in the α and β parameters, the PEER cell survival results were shown to be in agreement with VHEE results from the ARES beamline at DESY, Hamburg, Germany. Evident in the survival trends, VHEE produced

Academic Editors: Dandan Zheng, Alexander Podgorsak and Olga Maria Dona Lemus

Received: 19 January 2026
Revised: 11 February 2026
Accepted: 13 February 2026
Published: 16 February 2026

more cell sparing in all cell lines compared to 2 Gy/s X-rays delivered on the IMBL, another beamline at the Australian Synchrotron. The results of the mouse cadaver irradiations showed that PEER can safely and efficiently irradiate small animals. **Conclusions:** The PEER beamline is shown to possess suitable capabilities, including real-time dosimetry, repeatable alignment, and linac diagnostics, rendering it suitable for future in vivo VHEE UHDR FLASH radiotherapy investigations.

Keywords: FLASH; UHDR; VHEE; ultra-high dose-rate; very high-energy electrons; MOS*kin*; dosimetry; medical physics; radiobiology; beamline

1. Introduction

When treating cancer with radiation, the overarching goal is to provide a sufficient therapeutic dose to the tumour while minimising the radiation dose to surrounding normal tissues [1]. A rapidly advancing modality aimed at reducing undesirable effects to the normal tissue is FLASH radiotherapy, defined as the delivery of a treatment at average dose-rates above 40 Gy/s [2,3]. However, this threshold was defined over 10 years ago, with recent studies suggesting that a more complex relationship between average dose-rates, instantaneous dose-rates, and the total time of delivery must be understood in order to reliably induce the FLASH effect [4–10]. It has also been observed that tissue sparing increases proportionally to dose when treatments are delivered as a single fraction, often in less than 200 ms [11–16]. With mounting in vivo evidence, the radiobiology community strives to uncover the biological mechanisms responsible for the differential damage between tumour and normal tissue [17]. As such, the exact mechanisms are, at the time of writing, not completely understood.

The FLASH effect has been observed for irradiations with X-rays, protons, and electrons [18–21], with the first pre-clinical human trial having occurred in 2018 [22]. The use of electrons is increasingly common, as they require less energy to accelerate, are more efficient compared to X-ray production [23], and can be easily steered and/or focused [24–26]. However, electrons of clinical energies, generally a maximum of 20 MeV, do not penetrate tissue deeply and are mostly used to treat superficial tumours. To reach tumours located deeper within the body, very-high-energy electrons (VHEEs; electrons with energy > 50 MeV) are being investigated [27–35]. While there are currently only a small group of VHEE facilities worldwide, the linear accelerators (linacs) within these facilities are, without modifications, capable of delivering average dose-rates many orders of magnitude greater than clinical linacs, well above the 40 Gy/s threshold for FLASH, with even greater instantaneous dose-rates. While the beam parameters vary between facilities, they are mostly all capable of delivering single pulse deliveries on nanosecond timescales [36–38]. Those that require multiple single bunch fractions to achieve relevant therapeutic doses are still capable of meeting the average dose-rates required for FLASH, with ultra-high instantaneous dose-rates [39]. Further, new facilities are currently in development [40], and significant research is being conducted to realise compact VHEE accelerators no larger than current clinical machines while retaining FLASH capabilities [41–44], as well as imaging capabilities [45]. However, many of these projects are still in the accelerator research and development phase, so current research requires access to suitable, existing facilities.

The Pulsed Energetic Electrons for Research (PEER) beamline at the Australian Nuclear Science and Technology Organisation (ANSTO) Australian Synchrotron (AS) has experienced rapid development in recent years, led by crucial dosimetry and beam diagnostics research [46,47], to transform it from a storage ring injector [48] into a dual-use

facility suitable for external users to conduct ultra-high dose-rate (UHDR) VHEE medical physics studies and small animal radiobiology research. PEER is available to external users during machine development periods once a month on average. While these previous investigations suggest repeatable and measurable deliveries of dose are possible, accurate biological results are deemed necessary as a true test of PEERs capabilities. To confirm a valid transformation and benchmark its suitability for such investigations, a series of cell irradiations were performed for three distinct cell lines, A549 (cancerous lung cells), T98G (glioblastoma cells), and MDCK (normal canine kidney cells). The same cell lines were also irradiated at the AS Imaging and Medical Beamline (IMBL), adjacent to PEER. In addition to a well characterised X-ray beam used for many cell and small animal investigations [49–52], IMBL features on-site cell laboratories and small animal husbandry facilities. By measuring the delivered doses at PEER in real time using previously validated Centre for Medical Radiation Physics (CMRP) MOS*kin* detectors [53], clonogenic cell survival was compared between the two modalities using the linear quadratic model (LQM). The results were also compared to the work of another group investigating the relative biological effectiveness (RBE) of VHEE at low average dose-rates with ultra-high instantaneous dose-rates using the 154 MeV Accelerator Research Experiment at the SINBAD (ARES) facility at DESY, Hamburg, for the A549 cell line [54]. Radiation dose-rate effects have been observed in vitro in the order of Gy/min [55] and 20–250 Gy/s previously at IMBL [50–52], but less is known at the MGy/s scale of the PEER VHEE beam. High dose-rates have been shown to both reduce the time for cellular repair and consume oxygen, reducing the amount of free radicals that damage DNA [17]. Different alpha/beta ratios and repair probabilities of tumour and normal cells indicate that these mechanisms do not affect all cells to the same extent, perhaps reducing normal tissue damage and destroying cancer cells as efficiently as with clinical dose-rates [3]. These underlying mechanisms of the FLASH effect are further complicated in vivo due to dependent systems and organs and unique properties and function of tissues [56].

This work, therefore, will provide a useful insight into the cell response to dose-rates well above those used clinically. The cell survival results also confirm the accurate dosimetric and diagnostic capabilities of PEER, demonstrating the facilities' suitability for future use in radiobiological investigations.

While cell survival investigations are a significant step in the development of PEER, the availability and ease of access to on-site animal husbandry facilities places it in a unique position relative to global VHEE facilities. To investigate the feasibility of irradiating small animals at PEER, a complimentary experiment was performed using fresh mouse cadavers supplied by IMBL from a previous experiment. Using these mice allows refinement of the procedure and understanding of any safety concerns before further animal use, in accordance with the three Rs of animal ethics (replacement, reduction, and refinement). The experiment was a 'dress rehearsal' designed to assess logistical constraints such as turn around time for irradiations (due to stricter entry requirements for PEER compared to X-ray beamlines), feasibility of animal positioning, and qualitative assessment of dose delivery to a defined target on the mouse using the existing tools developed for dosimetric investigations.

Combining cell survival results and investigating the suitability of on-site animal husbandry facilities provides confirmation that the transformation and development of PEER has been conducted successfully. This paper demonstrates the successful benchmarking of the PEER facility, confirming its suitability for the ultra-high dose-rate medical physics and radiobiology research required to advance understanding of the FLASH effect.

2. Materials and Methods

2.1. Cell Preparation and Clonogenic Assay

MDCK cells were obtained from the lab of the Targeted Nano-Therapies theme of CMRP at the University of Wollongong. T98G and A549 cells were obtained from Merck Life Science Pty Ltd. (Bayswater, VIC, Australia). All cell lines were maintained using T75 cm^2 flasks in complete Dulbecco's Modified Eagle Medium (DMEM) supplemented with 10% Foetal Bovine Serum (FBS) and 1% penicillin (5000 units/mL) and streptomycin (5000 µg/mL) (Gibco™, ThermoFisher Scientific Australia Pty Ltd., Scoresby, VIC, Australia). Cells were incubated at 37 °C in 5% CO_2. All cell lines were prepared for radiation according to the following method: Cells were harvested from the T75 cm^2 flasks using trypsin containing 0.05% EDTA (Gibco™, ThermoFisher Scientific) and counted. The cells were then centrifuged at 300 g for 5 min with the supernatant discarded and cell pellet resuspended in complete DMEM to a concentration of 1,000,000 cells/mL. This stock was distributed to polymerase chain reaction (PCR) tubes (0.2 mL) with 200,000 cells per tube. PCR tubes were centrifuged at 300 g to generate a cell pellet ready for irradiation. A cell pellet is necessary to target all cells for irradiation as the VHEE beam width is <5 mm. All PCR tubes were sealed and did not contain any headspace, with 2 replicates prepared for each cell line.

Following irradiation, the cell pellet was vortexed and 10,000 cells were diluted in complete DMEM and added to 6-well plates, with each well containing 2 mL complete DMEM. For each tube, 2–3 seeding values were used in triplicate. After cells were incubated at 37 °C in 5% CO_2 for 14 doubling times, the cells were fixed and stained with 80% ethanol and solution of 5% crystal violet (Sigma Aldrich®, Merck Life Science Pty Ltd., Bayswater, VIC, Australia) mixed in a ratio of 1:4. Plating efficiency was normalised to the average plating efficiency of the 0 Gy control. In handling outliers, the only exclusions were colonies that were over-crowded (>150 colonies) or low-density (<10 colonies) for statistical relevance. Surviving fraction was determined as the ratio of the number of colonies of the irradiated samples to the number of colonies in the 0 Gy control with the results fitted using the LQM [55].

2.2. Phantom Production

To hold PCR tubes containing cell cultures, in-house phantoms were designed and 3D-printed using fused deposition modeling and polylactic acid (PLA), a common additive manufacturing material used extensively in medical physics [57–59]. The total thickness of the phantom was 20 mm, with the PCR tubes located centrally at 10 mm depth. To avoid regions of air around the PCR tubes, the exact dimensions were used to design slots for the tubes while maintaining sufficient distance between tubes to avoid overlapping irradiations. A channel was placed immediately behind to allow a MOS*kin* detector to be used during irradiations. The sensitive volume of the MOS*kin*s are aligned laterally with the tips of the PCR tubes, allowing for the plastic thickness, to confirm the dose experienced by the cells in real-time, as they have been spun down into the tip of the tube. Figure 1 shows the phantoms installed at the PEER end-station. The cross hairs drawn for alignment are highlighting physical marks placed during the manufacture of the phantom, so that positioning accuracy is only limited by the resolution of the stages and 3D printing process. A similar phantom was also manufactured without positions for PCR tubes, to allow for reference dosimetry with MOS*kin*s at the same depth of the PCR tubes during the initial beamline setup.

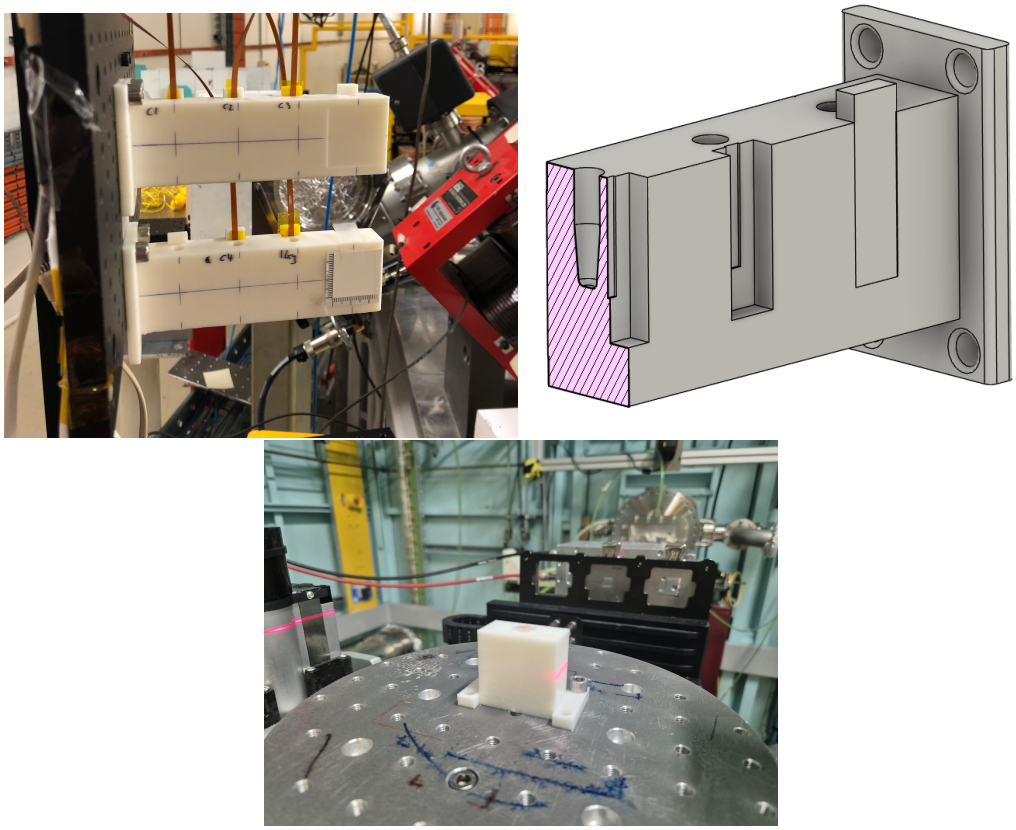

Figure 1. The 3D printed phantoms installed at PEER (**top**) and IMBL (**bottom**). Also shown is a cross-section from the 3D modeling of the PEER phantom, displaying the colocation of PCR tubes and MOS*kin* detectors for real-time dosimetry. The total thickness of both PEER and IMBL phantoms is 20 mm, with the PCR tubes located at 10 mm depth.

A further two phantoms were produced to allow irradiations at IMBL. Again using PLA, with the same total thickness and central positioning of the PCR tubes, one was produced to hold a 31022 PinPoint ionisation chamber (PTW Freiburg, Breisgau, Germany) for the purpose of reference dosimetry and another to hold a single PCR tube. The two phantoms were manufactured in such a way that the PinPoint sensitive volume and the location of the cells in the bottom of the PCR tube were at the same lateral position, relative to the beam center. This allowed the reference phantom to be used not only for confirming the dose, but for determining the required spatial coordinates of the stage, before swapping to the PCR phantom and irradiating the cell samples individually.

As PEER and IMBL are vastly different irradiation fields, the suitability of PLA was considered. In the case of 100 MeV electrons at PEER, liquid water was not an option when using real-time electronic dosimetry. While a commercial product such as Solid Water RMI457 (Gammex-RMI, Middleton, WI, USA) was considered, the ratio of mass collisional stopping powers between PLA and Solid Water is near unity, with a value of 0.973, calculated with values from the NIST E-Star database [60]. For the low-energy X-rays of IMBL, RMI457 has been previously shown to exhibit a difference in measured attenuation co-efficients as high as 8.77% relative to water, whereas PLA was within 5% [57]. For these reasons, the PLA was deemed suitable for comparison between the two facilities while also presenting a cost-effective and highly efficient manufacturing process allowing intricate designs that bulk machining may not achieve, and quick iterations of designs during the planning phase of the experiments.

2.3. Dosimetry and Cell Irradiations at PEER

As a standard procedure at PEER, the linac was first checked for stable charge delivery over a range of settings using a custom Faraday cup (FC), designed for PEER [47]. This data is then used to calibrate a fast current transformer for diagnostic purposes during the rest of the beam time. The FC data is recorded during further irradiations, so that it can be used as a secondary measure of relative charge stability throughout the experiment, though, of course, magnitudes are lower when other equipment is positioned between the device and the linac exit foil.

After the range of linac operating parameters had been determined, the reference phantom was installed on the linear stages with a scintillating screen fixed to an end. The scintillator was used to find and mark the central axis of the electron beam using in-house camera software, after which the alignment markers on the phantom were used to determine and store the stage positions for each MOS*kin* sensitive volume. This method has been used previously at PEER and shown to produce highly accurate, repeatable alignment within ±100 µm [53]. To determine the linac settings that would produce the desired doses within the phantom, the MOS*kin*s were placed within the reference phantom and irradiated with single, 200 ns pulses consisting of varied levels of charge. A single pulse consisted of 100 bunches, with a bunch length 100 ps, and a 2 ns spacing. Adjusting the total charge within the single pulse deliveries allowed for varied dose per pulse (DPP) corresponding to average dose-rates up to 10^7 Gy/s and instantaneous dose-rates up to 10^8 Gy/s. Much higher dose-rates are available at PEER, by increasing the total charge (which increases the dose), or by delivering the same total charge over a reduced number of bunches. However, 100 bunch pulses were chosen to ensure stability during this work as this was a well understood working point.

The cell phantoms produced to contain PCR tubes were then mounted on the linear stages. The PCR tubes were inserted, with MOS*kin*s placed directly behind, and irradiated. This quality assurance (QA) dosimetry confirmed the dose delivered during each cell exposure, rather than relying solely upon the results of the reference dosimetry. While pulse-to-pulse stability has been previously shown to be stable at PEER (it was not explicitly measured during this beam time but was evident during initial setup), and alignment very repeatable, if a PCR tube was misaligned to the beam or a pulse was delivered incorrectly, the MOS*kin* measurement would reveal this error. The MOS*kin* sensitive volume occupies a ring of 250 µm diameter, smaller than the tip of the PCR tube; hence, any uncertainty in the fabrication process still places the measurement within the region of interest.

During the first of three beam times, the A549 cell line was irradiated. A calculated estimate of the MOS*kin* sensitivity for 100 MeV electrons from previous film measurements was used to estimate the dose delivered for each level of pulse charge. During this first beam time, experiments were also conducted to accurately determine the sensitivity of the MOS*kin*, to be used retrospectively to determine the true doses. An unexpected outcome of this beam time was the discovery of a dose-rate dependence of Gafchromic™ EBT-XD (Ashland ECC) film [53], a phenomenon that has also been observed by other research groups for both electrons and protons [61–63]. At the time of writing, the cause of this dose-rate dependence is unknown and efforts are underway to understand the mechanism responsible. This meant that the doses received by A549 cells were lower than originally intended as the EBT-XD film was used for initial MOS*kin* sensitivity estimations. The further two beamtimes were used to irradiate the T98G and MDCK cells.

2.4. Dosimetry and Cell Irradiations at IMBL

Initial characterisation of the IMBL beam adheres to a well developed protocol, whereby initial dosimetry is performed within a 100 × 100 × 100 mm^3 Solid Water®

HE (Gammex-RMI, Middleton, WI, USA) phantom. Measurements are taken with a 31022 PinPoint ionisation chamber (PTW Freiburg, Germany) which has been previously calibrated for the field, at 20 mm depth using a 20×20 mm^2 collimator. The X-ray beam was produced using a superconducting multipole wiggler operating at 1.4 T, and filtration of 0.45 mm graphene, $15\sqrt{2}$ mm HD graphite and $2\sqrt{2}$ mm Cu. This produced a beam with average energy of 72.8 keV and a dose-rate of 2.3 Gy/s. The IMBL beam was only ~1 mm in the vertical dimension; hence, to achieve the 20×20 mm^2 field, the target and the collimator are scanned through the beam. The scanning velocity determines the dose, if all other parameters are held constant. Further detail of this process can be found in a previous study [49].

With the beam characterised, the 3D-printed dosimetry phantom was mounted to the stage and the 31022 ionisation chamber was used to determine the scanning velocity required to produce the desired doses at the same depth as the PCR tubes. A dose of 0.99 Gy was achieved with a scanning velocity of 2.63 mm/s. Further required doses are achieved by linear scaling of the velocity, inversely proportional to dose. Once the required parameters were determined and confirmed by measurement, the PCR phantom seen in Figure 1 was mounted and the cells were irradiated.

2.5. Mouse Cadaver Dress Rehearsal

To assess the feasibility of future in vivo experiments, particularly in the context of the anaesthesia time requirements for such work, fresh cadavers of 14 female C567BL/6 mice were used from the IMBL facility (animal ethics AS2023_02). In groups of two, the mice were euthanised with Lethabarb® and then transported to the PEER beamline once death had been confirmed. To assess the time required to successfully treat a mouse at PEER, the time of death was recorded to represent the start of the stable state of anesthesia, in which transport into the beam line and positioning can take place in a live animal experiment. As shown in Figure 2, they were mounted on a frame designed to hold both mice, with sufficient distance that there was no dose delivered to a mouse while it was out of field (previous work with dosimetry film has confirmed out of field dose to be negligible, within the noise level of unexposed film). Again using a scintillator to determine the beam location, the mice were aligned to a stick on target placed over their brain, with a point marked at random, simulating a true live animal treatment. Pieces of dosimetry film were also placed at the exit of the frame, to visually confirm the alignment had been successful. These films were not quantified for dose as the exit position of the frame is in-air, rather than a meaningful measurement in tissue. After exposure, the mice were transported back to the IMBL animal facilities and the time of arrival recorded.

IMBL has an established history of small animal radiobiological research; therefore, the same process was performed at IMBL to assess the difference in elapsed time between the two facilities. An existing frame (of which the PEER setup was based upon), shown in Figure 3, was used to hold and align the mice within the IMBL beam. The alignment and subsequent irradiation of mice within the beam was performed in the same manner as the cell irradiations, a standard and well refined procedure at IMBL.

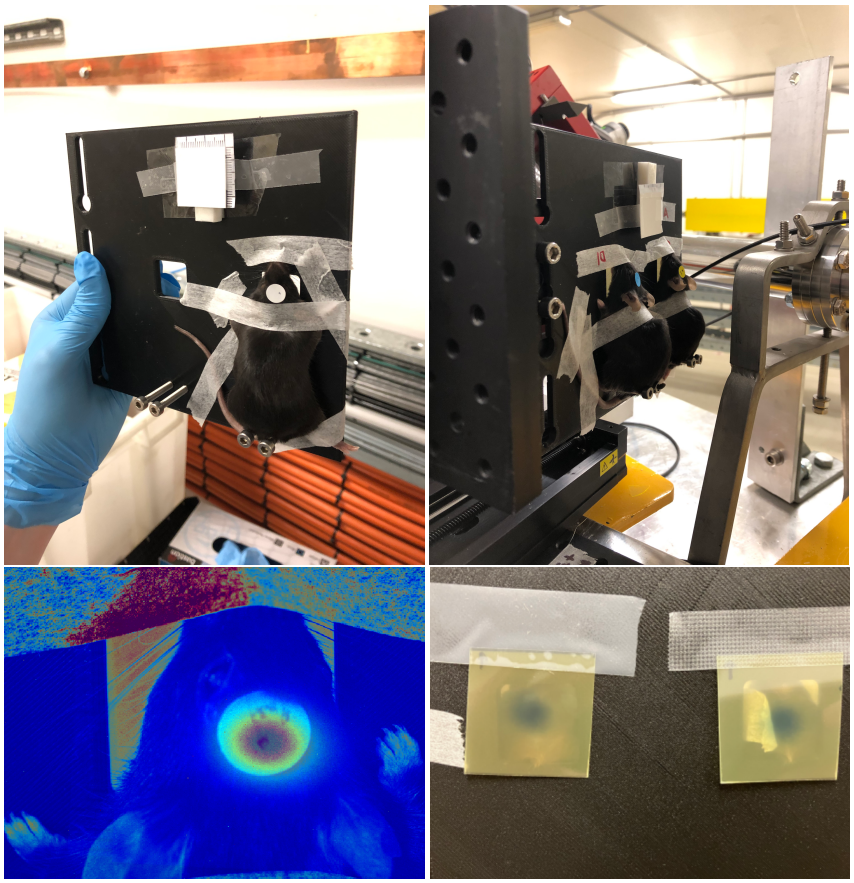

Figure 2. Top: The mouse irradiation apparatus setup at PEER. This is the first prototype, based upon existing designs used at IMBL. **Bottom left**: The visible beam spot from the alignment scintillator is superimposed onto a mouse image from irradiation to demonstrate the alignment method, with the dot in the centre of the sticker visible. **Bottom right**: Exit films confirm the intended targets were irradiated.

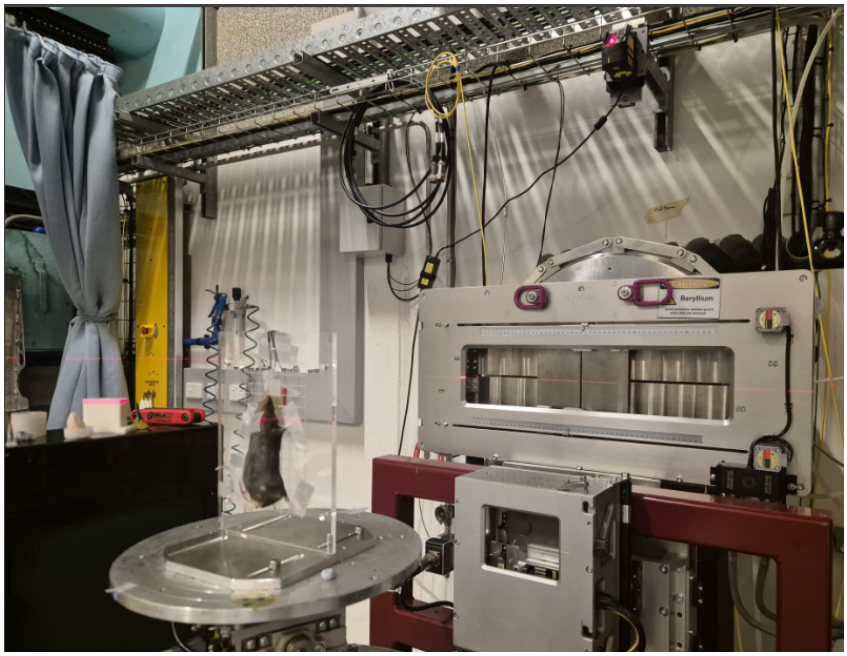

Figure 3. The mouse irradiation apparatus setup at IMBL. The X-ray beam enters from the back wall through a beryllium foil seen to the right of the image.

https://doi.org/10.3390/cancers18040640

3. Results

3.1. Cell Survival

Figure 4 shows the experimental data and the LQM survival curves for the three cell lines used in this study: A549, T98G, and MDCK. The A549 cell line has also been investigated at the ARES beamline, DESY, Hamburg [54]. Good agreement can be seen between ARES and PEER, noting that the ARES irradiations to determine VHEE RBE were performed using a beam scanning method, and while instantaneous dose-rates were as high as 2×10^{12} Gy/s, this resulted in average dose-rates of ~1.8 Gy/s, orders of magnitude lower than PEER at a maximum average dose-rate of ~3×10^{7} Gy/s during this study. The highest instantaneous dose-rate at PEER was 6×10^{8} Gy/s. Table 1 contains the alpha and beta fit parameters for the LQM curves, and the results between PEER and ARES are within error. This highlights the accuracy of the MOS*kin* dosimetry and PEER diagnostics at these extreme dose-rates. When comparing the PEER results to IMBL, the LQM fit parameters and curves are largely within error; however, the low energy X-rays deliver a consistently greater biological impact to all cells, captured with the larger alpha for more radiosensitive cell lines like A549 and MDCK, and with beta for the radiation-resistant T98G.

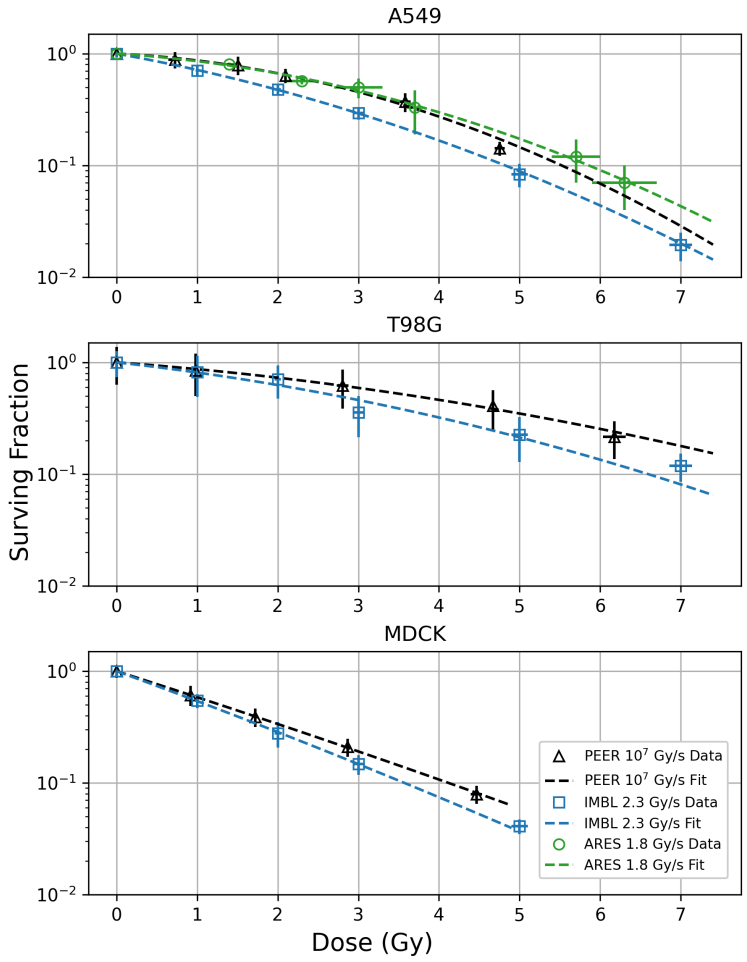

Figure 4. Clonogenic survival results for the investigated cell lines at PEER, IMBL, and ARES in the case of A549. The LQM has been fitted to the data for all cell lines. Good agreement can be seen between PEER and ARES. Data points indicate the mean surviving fraction compared to the 0 Gy plating efficiency and the quality assurance dose measurements made in real-time with the MOS*kin* detectors. Error bars represent the standard deviation of the mean. The raw data used to produce the ARES survival curve was obtained from [54], with the LQM refitted, resulting in the same fit parameters as the original work.

Table 1. The fitting parameters α and β of the LQM for each of the irradiations. The raw data representing the ARES results was obtained from [54].

Cell Line	α	β
A549		
PEER	0.080 ± 0.027	0.061 ± 0.010
ARES	0.10 ± 0.07	0.05 ± 0.03
IMBL	0.299 ± 0.008	0.037 ± 0.003
T98G		
PEER	0.122 ± 0.021	0.018 ± 0.005
IMBL	0.184 ± 0.065	0.025 ± 0.019
MDCK		
PEER	0.531 ± 0.006	0.007 ± 0.002
IMBL	0.606 ± 0.012	0.011 ± 0.006

3.2. Mouse Feasibility Study

The use of mouse cadavers allowed the testing of IMBLs animal husbandry facilities for suitability with experiments conducted on the PEER beamline. The closest IMBL facilities are approximately 60 m from the entrance to PEER, and with accelerator access requirements adding extra complexity, the time which a mouse must remain anesthetised was quantified. Table 2 contains the recorded times for PEER and IMBL irradiations, and it can be seen that there is minimal difference, with an average elapsed time of 43 min at PEER and 35 min at IMBL. The IMBL irradiations were performed by a single member of the group, as the labs, hutch, and operator station are immediately adjacent. PEER irradiations employed a team of four to minimise time delays due to transporting mice to and from the linac, the accelerator entrance requirements, and the distance to the AS Control Room, where PEER is currently operated from. The dominant contribution to elapsed times at PEER is the use of keyed safety interlocks, as the master key located in the control room must be brought to the accelerator tunnel entrance and inserted before team members can be assigned a personal key and enter PEER. For IMBL, however, like many synchrotron X-ray beamlines, the shutters are closed on the neighbouring control station and access to the hutch is then gained with the push of a button. It was determined during this investigation that for future experiments at PEER, only three personnel are required to complete such work.

Table 2. The times at which a mouse was euthanised, irradiated, and returned to the lab, demonstrating the intervals required to anaesthetise and irradiate a live mouse for treatment at PEER and IMBL.

Mouse ID	Time of Death	Irradiation Time	Return Time	Minutes Elapsed
PEER				
8	16:09	16:32	16:50	41
12	16:10	16:31	16:50	40
10	16:49	17:21	17:32	43
7	16:48	17:23	17:32	44
17	17:40	18:03	18:22	42
14	17:40	18:04	18:22	42
13	18:24	18:50	19:10	46
16	18:24	18:51	19:10	46
			Average	43

Table 2. *Cont.*

Mouse ID	Time of Death	Irradiation Time	Return Time	Minutes Elapsed
IMBL				
25	11:30	11:50	12:04	34
29	11:30	11:57	12:10	40
28	12:24	12:42	12:56	32
26	12:27	12:48	13:03	36
27	12:44	13:05	13:19	35
30	13:14	13:33	13:47	33
			Average	35

4. Discussion

This study demonstrated the capability of the PEER beamline for cell and animal research and provides further data on in vitro responses to VHEE and UHDR. The design of custom PCR tube phantoms allowed not only the irradiation of the cells at depth within a tissue equivalent material but also co-location of MOS*kin* detectors. As previously demonstrated, the capability of these detectors to provide real-time results [46,53] allowed accurate verification of the true dose delivered to the cells. While the PEER linac produces stable irradiations with very good repeatability, a reliable QA dosimetry system provides confidence both during and after a beam time.

A549 cell survival results on PEER provided further validation of the setup, showing good agreement with the VHEE results at ARES, despite differences in beam delivery (ARES uses an average dose-rate of 1.8 Gy/s and instantaneous dose-rate of 2×10^{12} Gy/s). The close agreement in the in vitro survival under similar conditions benchmarks the PEER in vitro setup and dosimetry. This foundation allowed investigation of more cell lines for any differences in cell survival due to 10^7 Gy/s VHEE compared to X-rays at 2.3 Gy/s. Overall, greater sparing was observed from PEER irradiations on all cell lines (MCDK, A549, and T98G) compared to irradiation with IMBL 2.3 Gy/s X-rays, seen with statistical significance in the alpha term of the LQM. However, individual data points were within the experimental error.

The results are limited by irradiation conditions, namely oxygenation, dose-rate saturation, and differences in beam LET. With a 10^7-fold increase in dose-rate for VHEE irradiations, one could expect more oxygen consumption and lower production of free radicals that cause damage to DNA [64]. This is known to promote more cell sparing, as perhaps indicated in our results; however, by irradiating cells in sealed PCR tubes, there is some degree of hypoxia, unlike in other techniques in open cell culture dishes or flasks. Thus, oxygenation effects may not greatly distinguish IMBL and PEER irradiations in our setup depending on the remaining oxygen concentration in the cell medium.

Despite the significant dose-rate escalation with VHEE, this did not produce additional cell death either, as seen previously with 9L gliosarcoma cells at IMBL [50]. The inability of cells to repair radiation damage delivered in a short time has also been observed in other cell lines in the range of 1.6–150 cGy/s [55]. This could indicate that the 2.3 Gy/s IMBL irradiation may already be above the dose-rate threshold for DNA repair in these cell lines and that there is little more to be gained with 10^7 Gy/s.

Lastly, the RBE of differing radiation types is known to be proportional to the linear energy transfer (LET) of the electron spectrum [65–68] and inversely proportional to energy within the relevant region. While the average LET of the secondary electron spectrum of IMBL X-rays is not precisely known, the range of LET from 250 kVp to 30 kVp X-rays in water is 2.0–3.6 keV/µm [69], whereas for 100 MeV electrons in water, the LET is 0.22 keV/µm [60,70,71]. From this, we can also expect more cell survival with PEER due to

the beam energy and a lower RBE, and the slight sparing observed in our results may be driven by this effect rather than the anticipated rapid consumption of oxygen.

The dose-rate phenomenon and FLASH effect both in cells in vitro and in vivo is complex, and precise mechanisms cannot yet be gleaned from this initial study of cell survival without further investigation. However, with access to tunable dose-rates at PEER, a deeper understanding of the cell response to radiation dose-rates can be uncovered, now with strong confidence in the PEER dosimetry and diagnostics suite, as well as the performance of the linac at the ultra-high dose-rates used within this investigation. More cell lines can therefore be investigated in future under different oxygenation conditions and variable dose-rates to better determine the dependence of cellular repair and oxygen consumption on radiation damage under ultra-high dose-rate FLASH conditions.

As VHEE radiotherapy progresses towards pre-clinical studies, suitable on-site animal husbandry facilities are a critical requirement. The use of IMBL's animal husbandry facilities in conjunction with PEER has been shown to be feasible, both from an animal welfare and logistical standpoint, as well as the suitability of the custom apparatus required to hold and align small animals at PEER. From the time of death to return of a mouse to the lab, a difference of only 8 min was measured at PEER relative to IMBL. The mice were successfully aligned and irradiated, with dosimetry film used at the exit surface to qualitatively confirm the alignment process. While two mice were mounted to the frame at PEER simultaneously, irradiating single mice would not change this time; rather it would simply lengthen the total number of hours required on the beamline. To expand this suitability to larger animals will be mostly a logistical exercise involving a different experimental table and linear stage setup at the PEER end-station. A caveat to this, however, is that access to PEER involves crossing over the synchrotron storage ring via stairs, so the weight of the animal being transported will eventually become an important consideration. By assessing the suitability with mouse cadavers, studies with live animals are deemed possible and will be explored in the near future. Doing so is an important step for the field of VHEE radiotherapy, especially at ultra-high dose-rates, so that the presence of an in vivo FLASH effect can be assessed and the beam parameters required to induce it can be investigated in detail. While instantaneous dose-rates at PEER will always be much higher than clinical linacs, previous work has shown that average dose-rates similar to that of clinical treatments can be achieved alongside the ultra-high average dose-rates of single pulse deliveries [53]. Such a large range of average dose-rates, combined with variable instantaneous dose-rates enables investigations to be conducted in both conventional and the ultra-high average dose-rate regimes expected to induce FLASH, on the same accelerator. Doing so will allow many parameters to be held constant while temporal effects are investigated.

The doses for all irradiations at PEER in this work were measured in real time using MOS*kin* detectors (IMBL irradiations adhered to an existing, well defined protocol). As with all solid state detectors, their use required initial calibration for the energy spectrum at PEER; however, no dose-rate or DPP dependence has been observed. Displaying excellent linearity to increasing DPP, MOS*kin*s are applicable for cellular and emerging pre-clinical work on VHEE accelerators. Used clinically to measure 70 µm skin dose and confirm the delivery against treatment planning systems, MOS*kin* detectors will be used in future work with live animals to confirm entrance and/or exit doses in real-time. A Monte Carlo model (Geant4) is currently being refined to be used for treatment planning in the absence of commercial offerings for novel VHEE treatment fields.

5. Conclusions

As an accelerator originally commissioned solely as an injector for the storage ring of the ANSTO AS, the PEER beamline has experienced rapid development. Through the design and commissioning of in-house diagnostics, combined with dose-rate independent MOS*kin* dosimetry, accurate and repeatable radiation delivery has been achieved. Particularly, MOS*kin* dosimetry allows real-time confirmation during every exposure, rather than reliance upon delayed methods such as dosimetry films. With these systems in place, the PEER beamline was benchmarked for in vitro and in vivo radiotherapy research by comparing cell survival results to low-energy, low-dose-rate X-ray irradiations at IMBL and low dose-rate VHEE results from an external group, with good agreement. Further, mouse cadavers were used to assess the suitability and predict logistical outcomes for live animal experiments. The results within this paper confirm that PEER is a suitable facility for future VHEE UHDR FLASH radiotherapy studies, both in the context of dosimetry and diagnostics, as well as necessary biological investigations.

Author Contributions: Conceptualisation, J.C.; methodology, J.C., E.E. and Y.-R.E.T.; software, P.B. and Y.-R.E.T.; validation, J.C. and E.E.; formal analysis, J.C. and E.E.; investigation, J.C., E.E., T.C., K.R., S.K. and Y.-R.E.T.; resources, M.W., K.B., M.C., D.H., M.T., E.S., A.R., Y.-R.E.T. and M.L.; data curation, J.C., and E.E.; writing—original draft preparation, J.C. and E.E.; writing—review and editing, J.C., E.E., T.C., K.R., M.W., K.B., E.G., M.T., E.S., Y.-R.E.T. and M.L.; visualisation, J.C.; supervision, E.G., A.R., Y.-R.E.T. and M.L.; project administration, J.C.; funding acquisition, J.C., Y.-R.E.T. and M.L. All authors have read and agreed to the published version of the manuscript.

Funding: J.C. and K.R. receive Australian Government RTP scholarships. J.C. was supported by an AINSE Ltd. Postgraduate Research Award (PGRA).

Institutional Review Board Statement: The animal study protocol was approved by the ANSTO Australian Synchrotron Animal Ethics Committee agreement AS2023_02.

Data Availability Statement: The raw data supporting the conclusions of this article will be made available by the authors on request.

Acknowledgments: This research was undertaken on the PEER and IMBL beamlines, Australian Synchrotron, part of ANSTO. The authors would like to thank the operators of the Australian Synchrotron.

Conflicts of Interest: A.R. and M.L. declare consulting with Electrogenics Laboratories Ltd., which is commercialising the MOS*kin* detector. Electrogenics Laboratories Ltd. had no role in the design of the study, in the collection, analyses, or interpretation of data, in the writing of the manuscript, or in the decision to publish the results.

Abbreviations

The following abbreviations are used in this manuscript:

VHEEs	Very-high-energy electrons
Linac	Linear accelerator
PEER	Pulsed Energetic Electrons for Research
UHDR	Ultra-high dose-rate
AS	ANSTO Australian Synchrotron
IMBL	Imaging and Medical Beamline
CMRP	Centre for Medical Radiation Physics
LQM	Linear quadratic model
RBE	Relative biological effectiveness
ARES	Accelerator Research Experiment at SINBAD
DMEM	Dulbecco's Modiefied Eagle Medium
FBS	Foetal Bovine Serum

PCR	Polymerase chain reaction
PLA	Polylactic acid
FC	Faraday cup
DPP	Dose per pulse
QA	Quality assurance
LET	Linear energy transfer

References

1. Metcalfe, P.; Kron, T.; Hoban, P.; Cutajar, D.; Hardcastle, N. *The Physics of Radiotherapy X-Rays and Electrons*, 3rd ed.; Medical Physics Publishing: Madison, WI, USA, 2007.
2. Favaudon, V.; Caplier, L.; Monceau, V.; Pouzoulet, F.; Sayarath, M.; Fouillade, C.; Poupon, M.F.; Brito, I.; Hupé, P.; Bourhis, J.; et al. Ultrahigh Dose-Rate FLASH Irradiation Increases the Differential Response between Normal and Tumor Tissue in Mice. *Sci. Transl. Med.* **2014**, *6*, 245ra93. [CrossRef] [PubMed]
3. Vozenin, M.C.; Bourhis, J.; Durante, M. Towards Clinical Translation of FLASH Radiotherapy. *Nat. Rev. Clin. Oncol.* **2022**, *19*, 791–803. [CrossRef] [PubMed]
4. Vozenin, M.C.; Montay-Gruel, P.; Limoli, C.; Germond, J.F. All Irradiations That Are Ultra-High Dose Rate May Not Be FLASH: The Critical Importance of Beam Parameter Characterization and In Vivo Validation of the FLASH Effect. *Radiat. Res.* **2020**, *194*, 571–572. [CrossRef]
5. Kacem, H.; Almeida, A.; Cherbuin, N.; Vozenin, M.C. Understanding the FLASH Effect to Unravel the Potential of Ultra-High Dose Rate Irradiation. *Int. J. Radiat. Biol.* **2022**, *98*, 506–516. [CrossRef]
6. Karsch, L.; Pawelke, J.; Brand, M.; Hans, S.; Hideghéty, K.; Jansen, J.; Lessmann, E.; Löck, S.; Schürer, M.; Schurig, R.; et al. Beam Pulse Structure and Dose Rate as Determinants for the Flash Effect Observed in Zebrafish Embryo. *Radiother. Oncol.* **2022**, *173*, 49–54. [CrossRef]
7. Schüler, E.; Acharya, M.; Montay-Gruel, P.; Loo, B.W., Jr.; Vozenin, M.C.; Maxim, P.G. Ultra-High Dose Rate Electron Beams and the FLASH Effect: From Preclinical Evidence to a New Radiotherapy Paradigm. *Med. Phys.* **2022**, *49*, 2082–2095. [CrossRef] [PubMed]
8. Bourhis, J.; Montay-Gruel, P.; Gonçalves Jorge, P.; Bailat, C.; Petit, B.; Ollivier, J.; Jeanneret-Sozzi, W.; Ozsahin, M.; Bochud, F.; Moeckli, R.; et al. Clinical Translation of FLASH Radiotherapy: Why and How? *Radiother. Oncol.* **2019**, *139*, 11–17. [CrossRef]
9. Jansen, J.; Beyreuther, E.; García-Calderón, D.; Karsch, L.; Knoll, J.; Pawelke, J.; Schürer, M.; Seco, J. Changes in Radical Levels as a Cause for the FLASH Effect: Impact of Beam Structure Parameters at Ultra-High Dose Rates on Oxygen Depletion in Water. *Radiother. Oncol. J. Eur. Soc. Ther. Radiol. Oncol.* **2022**, *175*, 193–196. [CrossRef]
10. Lin, B.; Du, H.; Hao, X.; Liang, Y.; Xu, H.; Tang, W.; Li, J.; Zhang, Y.; Du, X.B. The Influence of Beam Parameters on FLASH Effect. *Front. Oncol.* **2025**, *15*, 1431700. [CrossRef]
11. Sesink, A.; Geyer, R.; Devanand, P.; Böhlen, T.T.; Soutter, L.; Moeckli, R.; Bailat, C.; Herrera, F.G.; Grilj, V. Decrease in Dose per Fraction Impairs the FLASH Sparing Effect in Murine Intestine Model. *Radiother. Oncol.* **2026**, *214*, 111262. [CrossRef]
12. Böhlen, T.T.; Germond, J.F.; Bourhis, J.; Vozenin, M.C; Ozsahin, E.M.; Bochud, F.; Bailat, C.; Moeckli, R. Normal Tissue Sparing by FLASH as a Function of Single Fraction Dose: A Quantitative Analysis. *Int. J. Radiat. Oncol. Biol. Phys.* **2022**, *114*, 1032–1044. [CrossRef] [PubMed]
13. Montay-Gruel, P.; Acharya, M.M.; Gonçalves Jorge, P.; Petit, B.; Petridis, I.G.; Fuchs, P.; Leavitt, R.; Petersson, K.; Gondré, M.; Ollivier, J.; et al. Hypofractionated FLASH-RT as an Effective Treatment against Glioblastoma That Reduces Neurocognitive Side Effects in Mice. *Clin. Cancer Res.* **2021**, *27*, 775–784. [CrossRef]
14. Schulte, R.; Johnstone, C.; Boucher, S.; Esarey, E.; Geddes, C.G.R.; Kravchenko, M.; Kutsaev, S.; Loo, B.W.; Méot, F.; Mustapha, B.; et al. Transformative Technology for FLASH Radiation Therapy. *Appl. Sci.* **2023**, *13*, 5021. [CrossRef] [PubMed]
15. Vozenin, M.C.; Hendry, J.H.; Limoli, C.L. Biological Benefits of Ultra-high Dose Rate FLASH Radiotherapy: Sleeping Beauty Awoken. *Clin. Oncol.* **2019**, *31*, 407–415. [CrossRef] [PubMed]
16. Ilina, A.; Thomas, W.S.; Cao, X.; Reed, M.S.; Jarvis, K.; van der Kogel, A.; van Asselt, N.; Culberson, W.S.; Pogue, B.W. FLASH Effect Is Diminished by Daily Fractionation of Electron RT in Mouse Skin. *Phys. Med. Biol.* **2025**, *70*, 235020. [CrossRef]
17. Rosini, G.; Ciarrocchi, E.; D'Orsi, B. Mechanisms of the FLASH Effect: Current Insights and Advances. *Front. Cell Dev. Biol.* **2025**, *13*, 1575678. [CrossRef]
18. Atkinson, J.; Bezak, E.; Le, H.; Kempson, I. The Current Status of FLASH Particle Therapy: A Systematic Review. *Phys. Eng. Sci. Med.* **2023**, *46*, 529–560. [CrossRef]
19. Lin, B.; Gao, F.; Yang, Y.; Wu, D.; Zhang, Y.; Feng, G.; Dai, T.; Du, X. FLASH Radiotherapy: History and Future. *Front. Oncol.* **2021**, *11*, 644400. [CrossRef]

20. Gao, F.; Yang, Y.; Zhu, H.; Wang, J.; Xiao, D.; Zhou, Z.; Dai, T.; Zhang, Y.; Feng, G.; Li, J.; et al. First Demonstration of the FLASH Effect with Ultrahigh Dose Rate High-Energy X-rays. *Radiother. Oncol.* **2022**, *166*, 44–50. [CrossRef]
21. Giannini, N.; Gonnelli, A.; Gadducci, G.; Puccini, P.; Cavalieri, A.; Masturzo, L.; Pensavalle, J.H.; Celentano, M.; Di Martino, F.; Di Cocco, F.; et al. FLASH Radiotherapy Enhances the Therapeutic Ratio in an Embryonic In Vivo Model of Pancreatic Carcinoma. *ACS Appl. Mater. Interfaces* **2025**, *17*, 63286–63295. [CrossRef]
22. Bourhis, J.; Sozzi, W.J.; Jorge, P.G.; Gaide, O.; Bailat, C.; Duclos, F.; Patin, D.; Ozsahin, M.; Bochud, F.; Germond, J.F.; et al. Treatment of a First Patient with FLASH-radiotherapy. *Radiother. Oncol.* **2019**, *139*, 18–22. [CrossRef]
23. Montay-Gruel, P.; Corde, S.; Laissue, J.A.; Bazalova-Carter, M. FLASH Radiotherapy with Photon Beams. *Med. Phys.* **2022**, *49*, 2055–2067. [CrossRef]
24. Whitmore, L.; Mackay, R.I.; Van Herk, M.; Jones, J.K.; Jones, R.M. Focused VHEE (very high energy electron) beams and dose delivery for radiotherapy applications. *Sci. Rep.* **2021**, *11*, 14013. [CrossRef]
25. Kokurewicz, K.; Brunetti, E.; Welsh, G.H.; Wiggins, S.M.; Boyd, M.; Sorensen, A.; Chalmers, A.J.; Schettino, G.; Subiel, A.; DesRosiers, C.; et al. Focused very high-energy electron beams as a novel radiotherapy modality for producing high-dose volumetric elements. *Sci. Rep.* **2019**, *9*, 10837. [CrossRef]
26. Lv, J.; Zhao, X.; Liu, J.; Wu, D.; Yang, G.; Kang, M.; Yan, X. Dose Rate Assessment of Spot-Scanning Very High Energy Electrons Radiotherapy Driven by Laser Plasma Acceleration. *J. Appl. Phys.* **2023**, *133*, 194901. [CrossRef]
27. Fischer, J.; Whitmore, L.; Desrosiers, C.; Sheehy, S.; Bazalova-Carter, M. Very High-Energy Electrons as Radiotherapy Opportunity. *Eur. Phys. J. Plus* **2024**, *139*, 728. [CrossRef]
28. Fischer, J.; Hart, A.; Bedriová, N.; Krim, D.E.; Clements, N.; Bateman, J.; Korysko, P.; Farabolini, W.; Rieker, V.; Corsini, R.; et al. Spatially Fractionated Radiotherapy with Very High Energy Electron Pencil Beam Scanning. *Phys. Med. Biol.* **2025**, *70*, 015011. [CrossRef]
29. Böhlen, T.T.; Germond, J.F.; Traneus, E.; Bourhis, J.; Vozenin, M.C.; Bailat, C.; Bochud, F.; Moeckli, R. Characteristics of Very High-Energy Electron Beams for the Irradiation of Deep-Seated Targets. *Med. Phys.* **2021**, *48*, 3958–3967. [CrossRef]
30. Böhlen, T.T.; Germond, J.F.; Desorgher, L.; Veres, I.; Bratel, A.; Landström, E.; Engwall, E.; Herrera, F.G.; Ozsahin, E.M.; Bourhis, J.; et al. Very High-Energy Electron Therapy as Light-Particle Alternative to Transmission Proton FLASH Therapy—An Evaluation of Dosimetric Performances. *Radiother. Oncol.* **2024**, *194*, 110177. [CrossRef] [PubMed]
31. Sarti, A.; De Maria, P.; Battistoni, G.; De Simoni, M.; Di Felice, C.; Dong, Y.; Fischetti, M.; Franciosini, G.; Marafini, M.; Marampon, F.; et al. Deep Seated Tumour Treatments with Electrons of High Energy Delivered at FLASH Rates: The Example of Prostate Cancer. *Front. Oncol.* **2021**, *11*, 777852. [CrossRef] [PubMed]
32. Ronga, M.G.; Cavallone, M.; Patriarca, A.; Leite, A.M.; Loap, P.; Favaudon, V.; Créhange, G.; De Marzi, L. Back to the Future: Very High-Energy Electrons (VHEEs) and Their Potential Application in Radiation Therapy. *Cancers* **2021**, *13*, 4942. [CrossRef] [PubMed]
33. Bazalova-Carter, M.; Qu, B.; Palma, B.; Hårdemark, B.; Hynning, E.; Jensen, C.; Maxim, P.G.; Loo, B.W., Jr. Treatment Planning for Radiotherapy with Very High-Energy Electron Beams and Comparison of VHEE and VMAT Plans. *Med. Phys.* **2015**, *42*, 2615–2625. [CrossRef]
34. Franciosini, G. External Beam Radiotherapy with Electrons of Low (IOeRT) and High (VHEE) Energies: Status and Prospects for Conventional and FLASH Irradiations. *Nuovo Cimento Della Soc. Ital. Di Fis. C* **2024**, *47*. [CrossRef]
35. Panaino, C.; Piccinini, S.; Andreassi, M.; Bandini, G.; Borghini, A.; Borgia, M.; Di Naro, A.; Labate, L.; Maggiulli, E.; Portaluri, M.; et al. Very High-Energy Electron Therapy toward Clinical Implementation. *Cancers* **2025**, *17*, 181. [CrossRef] [PubMed]
36. Corsini, R.; Aksoy, A.; Farabolini, W.; Gilardi, A.; Malyzhenkov, A.; Bateman, J.; Dosanjh, M.; Korysko, P.; Robertson, C.; Rieker, V. Medical Activities in Clear: Studies towards Radiotherapy Using Very High Energy Electrons (Vhee) in the Flash Regime. In Proceedings of the Linear Accelerator Conference, LINAC, Chicago, IL, USA, 25–30 August 2024; pp. 674–677. [CrossRef]
37. Subiel, A.; Moskvin, V.; Welsh, G.H.; Cipiccia, S.; Reboredo, D.; Evans, P.; Partridge, M.; DesRosiers, C.; Anania, M.P.; Cianchi, A.; et al. Dosimetry of Very High Energy Electrons (VHEE) for Radiotherapy Applications: Using Radiochromic Film Measurements and Monte Carlo Simulations. *Phys. Med. Biol.* **2014**, *59*, 5811. [CrossRef]
38. Bazalova-Carter, M.; Liu, M.; Palma, B.; Dunning, M.; McCormick, D.; Hemsing, E.; Nelson, J.; Jobe, K.; Colby, E.; Koong, A.C.; et al. Comparison of Film Measurements and Monte Carlo Simulations of Dose Delivered with Very High-Energy Electron Beams in a Polystyrene Phantom. *Med. Phys.* **2015**, *42*, 1606–1613. [CrossRef]
39. Burkart, F.; Aßmann, R.; Dinter, H.; Jaster-Merz, S.; Kuropka, W.; Mayet, F.; Vinatier, T. The ARES Linac at DESY. In Proceedings of the 31st International Linear Accelerator Conference, Liverpool, UK, 28 August–2 September 2022; pp. 691–694. [CrossRef]
40. Angal-Kalinin, D.; Boogert, S.; Jones, J.K. Potential of the CLARA Test Facility for VHEE Radiotherapy Research. *Front. Phys.* **2024**, *12*, 1496850. [CrossRef]
41. Giuliano, L.; Alesini, D.; Cardelli, F.; Carillo, M.; Chiadroni, E.; Coppola, M.; Cuttone, G.; Curcio, A.; De Gregorio, A.; Raddo, R.; et al. A Compact C-band FLASH Electron Linear Accelerator Prototype for the VHEE SAFEST Project. *Front. Oncol.* **2025**, *15*, 1516576. [CrossRef]

42. Barty, C.P.J.; Algots, J.M.; Amador, A.J.; Barty, J.C.R.; Betts, S.M.; Castañeda, M.A.; Chu, M.M.; Daley, M.E.; De Luna Lopez, R.A.; Diviak, D.A.; et al. Design, Construction, and Test of Compact, Distributed-Charge, X-band Accelerator Systems That Enable Image-Guided, VHEE FLASH Radiotherapy. *Front. Phys.* **2024**, *12*, 1472759. [CrossRef]
43. Li, H.; Zha, H.; Lin, X.; Gao, Q.; Liu, F.; Shi, J.; Chen, H. Design of a 100-MeV Compact VHEE Beam Line in Tsinghua University. *Front. Phys.* **2024**, *12*, 1496272. [CrossRef]
44. Effarah, H.; Reutershan, T.; Seggebruch, M.; Algots, M.; Amador, A.; Baulch, J.; Drayson, O.; Hartemann, F.; Hwang, Y.; Lagzda, A.; et al. Preparations for Ultra-High Dose Rate 25–90 MeV Electron Radiation Experiments with a Compact, High-Peak-Current, x-Band Linear Accelerator. *Radiat. Res.* **2025**, *203*, 223–235. [CrossRef]
45. Schütze, P.; Abel, A.; Burkart, F.; de Silva, L.M.S.; Dinter, H.; Dojan, K.; Herkert, A.; Jaster-Merz, S.; Kellermeier, M.J.; Kuropka, W.; et al. electronCT—An Imaging Technique Using Very-High Energy Electrons. *Front. Phys.* **2024**, *12*, 1454854. [CrossRef]
46. Cayley, J.; Tan, Y.R.E.; Petasecca, M.; Cutajar, D.; Breslin, T.; Rosenfeld, A.; Lerch, M. MOSkin Dosimetry for an Ultra-High Dose-Rate, Very High-Energy Electron Irradiation Environment at PEER. *Front. Phys.* **2024**, *12*, 1401834. [CrossRef]
47. Cayley, J.; Paino, J.; Guatelli, S.; Rosenfeld, A.; Lerch, M.; Tan, Y.R.E. Simulation and Commissioning of a Faraday Cup for Absolute Charge Measurements of Very High-Energy Electrons in-Air at PEER. *Front. Phys.* **2024**, *12*, 1448025. [CrossRef]
48. Leblanc, G.S.; Boland, M.J.; Tan, Y.R.E. The Australian Synchrotron Project Storage Ring and Injection System. In Proceedings of the 2004 European Particle Accelerator Conference, Lucerne, Switzerland, 5–9 July 2004.
49. Davis, J.A.; Engels, E.; Petasecca, M.; Paino, J.; Tehei, M.; Corde, S.; Stevenson, A.; Hausermann, D.; Guatelli, S.; Rosenfeld, A.; et al. X-TREAM Protocol for in Vitro Microbeam Radiation Therapy at the Australian Synchrotron. *J. Appl. Phys.* **2021**, *129*, 244902. [CrossRef]
50. Engels, E.; Li, N.; Davis, J.; Paino, J.; Cameron, M.; Dipuglia, A.; Vogel, S.; Valceski, M.; Khochaiche, A.; O'Keefe, A.; et al. Toward personalized synchrotron microbeam radiation therapy. *Sci. Rep.* **2020**, *10*, 8833. [CrossRef] [PubMed]
51. Engels, E.; Lerch, M.; Tehei, M.; Konstantinov, K.; Guatelli, S.; Rosenfeld, A.; Corde, S. Synchrotron activation radiotherapy: Effects of dose-rate and energy spectra to tantalum oxide nanoparticles selective tumour cell radiosentization enhancement. *J. Phys. Conf. Ser.* **2017**, *777*, 012011. [CrossRef]
52. Engels, E.; Forrester, H.B.; Trappetti, V.; Mouchemore, K.; Klein, M.; Sprung, A.H.; Brunt, K.; Barnes, M.J.; Cameron, M.; de Rover, V.; et al. Is Ultrahigh Dose Rate Critical for the Effectiveness of Microbeam Radiation Therapy in a Broad-Beam Combined Treatment? *Adv. Radiat. Oncol.* **2026**, *11*, 101949. [CrossRef]
53. Cayley, J.; Engels, E.; Charles, T.; Bennetto, P.; Cameron, M.; Poder, J.; Hausermann, D.; Paino, J.; Butler, D.; Cutajar, D.; et al. Establishing Linearity of the MOSkin Detector for Ultra-High Dose-per-Pulse, Very-High-Energy Electron Radiotherapy Using Dose-Rate-Corrected EBT-XD Film. *Appl. Sci.* **2025**, *15*, 8101. [CrossRef]
54. Wanstall, H.C.; Burkart, F.; Dinter, H.; Kellermeier, M.; Kuropka, W.; Mayet, F.; Vinatier, T.; Santina, E.; Chadwick, A.L.; Merchant, M.J.; et al. First in Vitro Measurement of VHEE Relative Biological Effectiveness (RBE) in Lung and Prostate Cancer Cells Using the ARES Linac at DESY. *Sci. Rep.* **2024**, *14*, 10957. [CrossRef]
55. Gordon Steel, G.; Deacon, J.M.; Duchesne, G.M.; Horwich, A.; Kelland, L.R.; Peacock, J.H. The dose-rate effect in human tumour cells. *Radiother. Oncol.* **1987**, *9*, 299–310. [CrossRef] [PubMed]
56. Limoli, C.L.; Vozenin, M.C. Reinventing Radiobiology in the Light of FLASH Radiotherapy. *Annu. Rev. Cancer Biol.* **2023**, *7*, 1–21. [CrossRef]
57. Bustillo, J.P.O.; Paino, J.; Barnes, M.; Cayley, J.; De Rover, V.; Cameron, M.; Engels, E.E.M.; Tehei, M.; Beirne, S.; Wallace, G.G.; et al. Design, Construction, and Dosimetry of 3D Printed Heterogeneous Phantoms for Synchrotron Brain Cancer Radiation Therapy Quality Assurance. *Phys. Med. Biol.* **2024**, *69*, 145003. [CrossRef] [PubMed]
58. Kim, S.Y.; Park, J.W.; Park, J.; Yea, J.W.; Oh, S.A. Fabrication of 3D Printed Head Phantom Using Plaster Mixed with Polylactic Acid Powder for Patient-Specific QA in Intensity-Modulated Radiotherapy. *Sci. Rep.* **2022**, *12*, 17500. [CrossRef]
59. Diaz-Merchan, J.A.; Español-Castro, C.; Martinez-Ovalle, S.A.; Vega-Carrillo, H.R. Bolus 3D Printing for Radiotherapy with Conventional PLA, ABS and TPU Filaments: Theoretical-experimental Study. *Appl. Radiat. Isot.* **2023**, *199*, 110908. [CrossRef]
60. NIST. NIST E-Star Database. Available online: https://physics.nist.gov/PhysRefData/Star/Text/ESTAR.html (accessed on 27 June 2024).
61. Del Sarto, D.; Masturzo, L.; Cavalieri, A.; Celentano, M.; Fuentes, T.; Gadducci, G.; Giannini, N.; Gonnelli, A.; Milluzzo, G.; Paiar, F.; et al. A Systematic Investigation on the Response of EBT-XD Gafchromic Films to Varying Dose-per-Pulse, Average Dose-Rate and Instantaneous Dose-Rate in Electron Flash Beams. *Front. Phys.* **2025**, *13*, 1474416. [CrossRef]
62. Villoing, D.; Koumeir, C.; Bongrand, A.; Guertin, A.; Haddad, F.; Métivier, V.; Poirier, F.; Potiron, V.; Servagent, N.; Supiot, S.; et al. Technical Note: Proton Beam Dosimetry at Ultra-High Dose Rates (FLASH): Evaluation of GAFchromic™ (EBT3, EBT-XD) and OrthoChromic (OC-1) Film Performances. *Med. Phys.* **2022**, *49*, 2732–2745. [CrossRef]
63. Yasuda, H.; Toshito, T.; Umezawa, M.; Yamada, M.; Tanaka, K.; Omachi, C.; Yogo, K.; Bantan, H.; Nakashima, T. Comparative Analysis of the Responses of EBT-XD and EBT4 Films to Ultra-High Dose Rate Proton Beams. *Radiat. Phys. Chem.* **2026**, *239*, 113349. [CrossRef]

64. Tinganelli, W.; Ma, N.Y.; Von Neubeck, C.; Maier, A.; Schicker, C.; Kraft-Weyrather, W.; Durante, M. Influence of acute hypoxia and radiation quality on cell survival. *J. Radiat. Res.* **2013**, *54*, i23–i30. [CrossRef]
65. BARENDSEN, G.W. Parameters of Linear-Quadratic Radiation Dose-Effect Relationships: Dependence on LET and Mechanisms of Reproductive Cell Death. *Int. J. Radiat. Biol.* **1997**, *71*, 649–655. [CrossRef]
66. McMahon, S.J. The Linear Quadratic Model: Usage, Interpretation and Challenges. *Phys. Med. Biol.* **2018**, *64*, 01TR01. [CrossRef] [PubMed]
67. Bistrović, M.; Bišćan, M.; Viculin, T. RBE of 20 kV and 70 kV X-rays Determined for Survival of V 79 Cells. *Radiother. Oncol.* **1986**, *7*, 175–180. [CrossRef]
68. Takatsuji, T.; Yoshikawa, I.; Sasaki, M.S. Generalized Concept of the LET-RBE Relationship of Radiation-Induced Chromosome Aberration and Cell Death. *J. Radiat. Res.* **1999**, *40*, 59–69. [CrossRef] [PubMed]
69. Vassiliev, O.N. On Calculation of the Average Linear Energy Transfer for Radiobiological Modelling. *Biomed. Phys. Eng. Express* **2021**, *7*, 015001. [CrossRef] [PubMed]
70. The International Commission on Radiation Units and Measurements (ICRU). *Stopping Powers for Electrons and Positrons*; Technical Report 0-913394-31-9—ICRU–37 INIS Reference Number: 24031395; ICRU: Bethesda, MA, USA, 1984.
71. Bichsel, H. *Stopping Power of Fast Charged Particles in Heavy Elements*; National Institute of Standards and Technology: Gaithersburg, MD, USA, 1991.